IEEE Access
Multidisciplinary | Rapid Review | Open Access Journal

Received November 12, 2021, accepted December 1, 2021, date of publication December 6, 2021,
date of current version December 13, 2021.

Digital Object Identifier 10.1109/ACCESS.2021.3132955

Pole-Zero Cancellation Speed Control With Variable Current Cut-Off Frequency for Servo Motors

SUNG HYUN YOU[1], YEON JI[2], AND SEOK-KYOON KIM[2]
[1]Department of Electronic Engineering, Chosun University, Gwangju 61452, South Korea
[2]Department of Creative Convergence Engineering, Hanbat National University, Daejeon 34158, South Korea

Corresponding author: Seok-Kyoon Kim (lotus45kr@gmail.com)

This work was supported in part by the Basic Science Research Program through the National Research Foundation of Korea (NRF) by the Ministry of Education under Grant 2018R1A6A1A03026005, and in part by the National Research Foundation of Korea (NRF) Grant by the Korean Government through the Ministry of Science and ICT under Grant NRF-2021R1C1C1004380 and Grant NRF-2020R1G1A1103036.

ABSTRACT This article presents a novel system parameter-independent double-loop solution to the speed control problem of servo motors incorporating the variable current cut-off frequency into the current-loop. The active damping terms for both the inner and outer loops make it possible to assign the pole-zero cancellation nature to the closed-loop system by cooperating the structured proportional-integral gains. The proposed analytic variable cut-off frequency mechanism automatically boosts the transient current-cut off frequency and decreases it to its initial value in the steady-state operation to secure the improved relative stability and reduced current ripple level, maintaining the rapid speed tracking behavior (feasibility of the high-speed cut-off frequency). The QUBE-servo2 kit experimentally verifies the practical benefits of the proposed solution.

INDEX TERMS Servo motor, speed control, current cut-off frequency, pole-zero cancellation, active-damping.

I. INTRODUCTION

Servo motors have been widely applied in applications such as home appliances, robotics, and mobility devices because of their high closed-loop performance and reasonable cost. This system adopted the DC motors (DCMs) as the mechanical part owing to the simple structure and low cost. As another version of DCMs, brushless DCMs (BLDCMs) have additional industrial applications because of their power efficiency improvement due to the removal of brush; however, they require additional algorithms because of the involvement of a three-phase inverter as the electrical driver part [1]–[5].

Speed servo motors with both the DCMs and BLDCMs require the single-loop for the speed feedback whose regulation can be achieved by the conventional proportional-integral (PI) controller. The approximated (ignoring the current dynamics) first-order open-loop transfer function from the stator voltage to the speed make it possible to implement this single-loop control strategy, which may limit the feasible speed cut-off frequency range owing to the ignorance of current dynamics [4], [6], [7]. For a high precision, the controller must involve the current-loop exhibiting a sufficiently high cut-off frequency for its transfer function, resulting in double and triple loops for speed and position servo applications, respectively [8]. The PI controller was preferred for implementing these multi-loop systems owing to its structural simplicity; this requires the additional gain scheduler (as in [9]) to enlarge the feasible operating region due to the load uncertainties. The feedback linearization controller made it possible to avoid the use of an additional gain scheduler by incorporating the parameter dependent feed-forward compensator and PI gain structure (leading to the pole-zero cancellation) [8], whose closed-loop precision level would be increased by adopting the additional online motor parameter identifiers as in [10]–[13].

Several novel solutions were based-on an adaptive, neural network, and back-stepping technique for improved closed-loop robustness against parameter and load variations [14], [15]. The DOB-based controller attempted to solve the parameter dependence problem under the

The associate editor coordinating the review of this manuscript and approving it for publication was Mou Chen.

double-loop strategy using a rigorous closed-loop stability analysis, where the combination of integral action and DOB considerably improves the closed-loop robustness [6]. As an advanced solution, the novel proportional-integral-derivative (PID) controller considerably improved the closed-loop robustness by incorporating numerical solver-dependent online self-tuning algorithms [16]. Another recent approach replaced the integrator with the nonlinear DOB while ensuring the offset-free nature and incorporating the online self-tuner (numerical optimization process-free), and magnifying the speed cut-off frequency in the control law [4]. The parameter-independent acceleration observer and surface stabilizer were systematically designed as subsystems for the DOB-based control law, including the active damping term [7], [17].

These extant solutions require the current cut-off frequency to be set as constant a constantly high-value covering the high speed cut-off frequency leading to the rapid speed-tracking behavior (high speed cut-off frequency). However, the high setting of current-cut off frequency results in the current ripple level magnification and relative stability degradation, which correspond to the challenge of this study. The proposed solution addresses this problem by introducing a variable cut-off frequency for the inner loop with the following three contributions:

1) a variable cut-off frequency mechanism for the inner loop in the analytic form to make the high speed cut-frequency feasible as lowering the steady-state current cut-off frequency value leading to the current ripple reduction and improved relative stability,
2) a pole-zero cancellation current controller including the nonlinear DOB for improving the accuracy of variable cut-off frequency system implementation for the inner loop, and
3) an outer loop pole-zero cancellation speed controller with the active damping term suppressing the external disturbances.

The experimental study justifies the merits of the proposed solution using the QUBE-servo2 hardware platform.

In the remainder of this paper, Section II briefly introduces the mechanical and electrical dynamics of the servo motor. Section III provides the proposed control algorithm with a block diagram for actual implementation. Section IV analyzes the closed-loop properties. Section V presents the experimental results. Finally, Section VI concludes the paper, future work.

II. SERVO MOTOR DYNAMICS

The stator current (i_a in A) and rotor speed (ω_m in rad/s) are considered as the state variables excited by the stator voltage (v_a in V) treated as the control input, which satisfies the second-order dynamic relationship:

$$J_m\dot{\omega}_m = -B_m\omega_m + T_e - T_L, \tag{1}$$
$$L_a\dot{i}_a = -R_a i_a - e_a + v_a, \ \forall t \geq 0, \tag{2}$$

with the output torque T_e (in Nm) and the back-electromotive force (EMF) term e_a (in V) being proportional to the current and speed as $T_e = k_T i_a$ and $e_a = k_e\omega_m$. Note that $k_T = k_e$ for the permanent magnet-type systems considered in this study. The load torque T_L (in Nm) functions as the mismatched external disturbance for this system. The two coefficients J_m (in kgm^2) and B_m (in Nm/rad/s) represent the rotor inertia and viscous damping effects. The resistance and inductance values for the stator coil are given by R_a (in Ω) and L_a (in H), respectively.

To handle the system parameter and load variation problems, the nominal coefficient values denoted as $(\cdot)_0$ for its true values $(\cdot)$ (e.g., $R_{a,0}$ for R_a) are introduced to rewrite the dynamic equations (1) and (2) as

$$J_{m,0}\dot{\omega}_m = -B_{m,0}\omega_m + k_{T,0}i_a + d_{\omega_m}, \tag{3}$$
$$L_{a,0}\dot{i}_a = -R_{a,0}i_a - k_{T,0}\omega_m + v_a + \bar{d}_{i_a}, \ \forall t \geq 0, \tag{4}$$

with unknown time-varying lumped disturbances d_{ω_m} and $\bar{d}_{i_a}$, which derive the proposed solution and beneficial closed-loop properties.

III. SPEED CONTROLLER

This study devises an advanced cascade-type stator voltage update rule to guarantee the closed-loop speed dynamics given in the low-pass filter (LPF) form:

$$\dot{\omega}_m^* = \omega_{sc}(\omega_{m,ref} - \omega_m^*), \ \forall t \geq 0, \tag{5}$$

with respect to the speed reference $\omega_{m,ref}$ and cut-off frequency $\omega_{sc}(= 2\pi f_{sc})$ in rad/s (outer loop), the maximum value of which is limited by the inner loop (current control) cut-off frequency, denoted as $\omega_{cc}(= 2\pi f_{cc})$ in rad/s. In summary, the control objective is constituted as the exponential convergence:

$$\lim_{t\to\infty} \omega_m = \omega_m^*, \tag{6}$$

where ω_m^* represents the desired input-output behavior (from the reference to the output) satisfying (5).

A. OUTER LOOP CONTROLLER

First, rewrite the open-loop speed dynamics (5) as

$$J_{m,0}\dot{\omega}_m = -B_{m,0}\omega_m + k_{T,0}i_{a,ref} - k_{T,0}\tilde{i}_a + d_{\omega_m}, \ \forall t \geq 0,$$

with the current reference $i_{a,ref}$ and its error $\tilde{i}_a = i_{a,ref} - i_a$, whose stabilization can be accomplished by the proposed pole-zero cancellation control law:

$$i_{a,ref} = \frac{1}{k_{T,0}}((B_{m,0} - b_{d,sc})\omega_m + J_{m,0}\omega_{sc}\tilde{\omega}_m + b_{d,sc}\omega_{sc}\int_0^t \tilde{\omega}_m d\tau), \ \forall t \geq 0, \tag{7}$$

with the speed error $\tilde{\omega}_m = \omega_{m,ref} - \omega_m$ and active-damping parameter $b_{d,sc} > 0$ resulting in the pole-zero cancellation together with the control gain from above. For details, see Section IV.

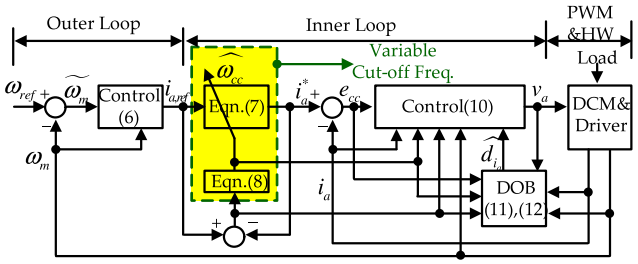

FIGURE 1. Control system configuration

B. INNER LOOP CONTROLLER

1) VARIABLE CUT-OFF FREQUENCY

Consider the first-order target current dynamics for given reference $i_{a,ref}$:

$$\dot{i}_a^* = \hat{\omega}_{cc}(i_{a,ref} - i_a^*), \ \forall t \geq 0, \tag{8}$$

with the variable cut-off frequency $\hat{\omega}_{cc}$ driven by the proposed update rule:

$$\dot{\hat{\omega}}_{cc} = \gamma_{cc}((\tilde{i}_a^*)^2 + \rho_{cc}\tilde{\omega}_{cc}), \ \hat{\omega}_{cc}(0) = \omega_{cc}(> 0), \ \forall t \geq 0, \tag{9}$$

with the two design parameters $\gamma_{cc} > 0$ and $\rho_{cc} > 0$ and errors $\tilde{i}_a^* = i_{a,ref} - i_a^*$ and $\tilde{\omega}_{cc} = \omega_{cc} - \hat{\omega}_{cc}$ (e.g., i_a^* represents the desired current trajectory satisfying (8)). The target system (8) has the same structure as the LPF, except for the time-varying cut-off frequency $\hat{\omega}_{cc}$. Moreover, the time-varying cut-off frequency dynamics (9) makes the closed-loop stability issue non-trivial due to its nonlinearity $(\tilde{i}_a^*)^2$, which is formally analyzed in Section IV.

2) CURRENT CONTROLLER

The definition of current error $e_{cc} = i_a^* - i_a$ produces the dynamics:

$$L_{a,0}\dot{e}_{cc} = \phi_{cc} - v_a + d_{i_a}, \ \forall t \geq 0, \tag{10}$$

with $\phi_{cc} := L_{a,0}\dot{i}_a^* + R_{a,0}i_a + k_{T,0}\omega_m$, $d_{i_a} = -\bar{d}_{i_a}$, which can be stabilized by the proposed control law:

$$v_a = (b_{d,cc} + L_{a,0}k_{cc})e_{cc} + b_{d,cc}k_{cc}\int_0^t e_{cc}d\tau + \phi_{cc} + \hat{d}_{i_a}, \tag{11}$$

$\forall t \geq 0$, with the current error convergent rate $k_{cc} > 0$ and active-damping parameter $b_{d,cc} > 0$ resulting in the pole-zero cancellation together with the control gain form above. See Section IV for details. The DOB yields the estimated disturbance $\hat{d}_{i_a}$ according to the following rule:

$$\dot{z}_{i_a} = -l_{i_a}z_{i_a} - l_{i_a}^2 L_{a,0}e_{cc} + l_{i_a}(-\phi_{cc} + v_a), \tag{12}$$

$$\hat{d}_{i_a} = z_{i_a} + l_{i_a}L_{a,0}e_{cc}, \ \forall t \geq 0, \tag{13}$$

with gain $l_{i_a} > 0$. Fig. 1 presents the resulting control system configuration.

IV. ANALYSIS

A. INNER LOOP ANALYSIS

This section begins with the subsystem analysis in the inner loop, such as the target current dynamics (8), the variable cut-off frequency update rule (9), and DOB (12) and (13). First, Lemma 1 addresses the stability issue for the target current dynamics (8).

Lemma 1: The subsystem comprising (8)-(9) guarantees the exponential convergence

$$\lim_{t\to\infty} i_a^* = i_{a,ref}$$

as $\dot{i}_{a,ref} \to 0$ exponentially. ◊

Proof: The error dynamics for $\tilde{i}_a^* = i_{a,ref} - i_a^*$ and $\tilde{\omega}_{cc} = \omega_{cc} - \hat{\omega}_{cc}$, obtained by (8) and (9), transform the positive definite function

$$V_{vc} := \frac{1}{2}(\tilde{i}_a^*)^2 + \frac{1}{2\gamma_{cc}}\tilde{\omega}_{cc}^2 \tag{14}$$

into

$$\begin{aligned}\dot{V}_{vc} &= -\omega_{cc}(\tilde{i}_a^*)^2 - \rho_{cc}\tilde{\omega}_{cc}^2 + \dot{i}_{a,ref}\tilde{i}_a^* \\ &\leq -\alpha_{vc}V_{vc} + \dot{i}_{a,ref}\tilde{i}_a^*, \ \forall t \geq 0,\end{aligned}$$

with $\alpha_{vc} := \min\{2\omega_{cc}, 2\rho_{cc}\gamma_{cc}\}$. This concludes the $\mathcal{L}_2$-stability for the system $\dot{i}_{a,ref} \mapsto \tilde{i}_a^*$ due to its strict passivity [18]. Thus, the claim becomes true. ■

The results from Lemma 1 only show that the subsystem (9) continuously updates the variable cut-off frequency to the direction for the exponential convergence $i_a^* \to i_{a,ref}$. However, this is insufficient for discovering the variable cut-off frequency behavior. Lemma 2 proves that the update rule (9) guarantees the cut-off frequency boosting property from its initial value ω_{cc}.

Lemma 2: The time-varying cut-off frequency $\hat{\omega}_{cc}$ from the update rule (9) satisfies

$$\hat{\omega}_{cc} \geq \omega_{cc}, \ \forall t \geq 0. \tag{15}$$

◊

Proof: The solution to the update rule (9) can be obtained by its two-sided integration as

$$\begin{aligned}\hat{\omega}_{cc} = e^{-\gamma_{cc}\rho_{cc}t}\omega_{cc} \\ + \int_0^t e^{-\gamma_{cc}\rho_{cc}(t-\tau)}(\gamma_{cc}\rho_{cc}\omega_{cc} + \gamma_{cc}(\tilde{i}_a^*)^2)d\tau,\end{aligned}$$

whose lower bound can be easily obtained as $\hat{\omega}_{cc} \geq \omega_{cc}$, $\forall t \geq 0$. Thus, the claim comes true. ■

The resultant boosting property (15) increases the feasible speed cut-off frequency (f_{sc} Hz, $\omega_{sc} = 2\pi f_{sc}$ rad/s) range for a given initial current cut-off frequency f_{cc} ($\hat{\omega}_{cc}(0) = \omega_{cc} = 2\pi f_{cc}$) based on the desired cut-off frequency relationship $\omega_{cc} \geq 10\omega_{sc}$ (in [8]). Section V experimentally demonstrates this practical merit.

The DOB (12) and (13) does not explicitly show the estimated disturbance dynamics, which is derived by Lemma 3 by investigating the DOB output dynamics using the combination of (12) and (13).

Lemma 3: The estimated disturbance $\hat{d}_{i_a}$ from the DOB (12)-(13) satisfies

$$\dot{\hat{d}}_{i_a} = l_{i_a}(d_{i_a} - \hat{d}_{i_a}),\ \forall t \geq 0. \tag{16}$$

♢

Proof: From the DOB output (13), it holds that (using (12))

$$\begin{aligned}\dot{\hat{d}}_{i_a} &= \dot{z}_{i_a} + l_{i_a}L_{a,0}\dot{e}_{cc}\\ &= -l_{i_a}(\hat{d}_{i_a} - l_{i_a}L_{a,0}e_{cc}) - l_{i_a}^2L_{a,0}e_{cc}\\ &\quad +l_{i_a}(-\phi_{cc} + v_a) + l_{i_a}L_{a,0}\dot{e}_{cc}\\ &= l_{i_a}(L_{a,0}\dot{e}_{cc} - \phi_{cc} + v_a - \hat{d}_{i_a}) = l_{i_a}(d_{i_a} - \hat{d}_{i_a}),\end{aligned}$$

$\forall t \geq 0$, with the application of relationship (10), which verifies the result of this lemma. ■

Lemma 4 shows the inherent pole-zero cancellation characteristic of the inner loop.

Lemma 4: The proposed controller (11) forces the inner loop dynamics to be the first-order system:

$$\dot{e}_{cc} = -k_{cc}e_{cc} + \tilde{d}_{i_a,F} + \tilde{d}_{i_a}, \tag{17}$$

with the filtered signal $\tilde{d}_{i_a,F}$ such that

$$\dot{\tilde{d}}_{i_a,F} = -c_1\tilde{d}_{i_a,F} - c_2\tilde{d}_{i_a},\ \forall t \geq 0, \tag{18}$$

$\forall t \geq 0$, for some positive constants c_i, $i = 1, 2$, where $\tilde{d}_{i_a} := d_{i_a} - \hat{d}_{i_a}$. ♢

Proof: The substitution of the control law (11) into the current error dynamics (10) produces the state-space representation for the state $\boldsymbol{x}_{i_a} := \begin{bmatrix} e_{cc} & \sigma_{i_a}\end{bmatrix}^T$ ($\sigma_{i_a} := b_{d,cc}k_{cc}\int_0^t e_{cc}d\tau$) and output $y_{i_a} = e_{cc}$ as

$$\begin{aligned}\dot{\boldsymbol{x}}_{i_a} &= \boldsymbol{A}_{i_a}\boldsymbol{x}_{i_a} + \boldsymbol{b}_{i_a}r + \boldsymbol{b}_{d_{i_a}}\tilde{d}_{i_a},\\ y_{i_a} &= \boldsymbol{c}_{i_a}\boldsymbol{x}_{i_a},\ \forall t \geq 0,\end{aligned}$$

with $\boldsymbol{A}_{i_a} := \begin{bmatrix} -\frac{(b_{d,cc}+L_{a,0}k_{cc})}{L_{a,0}} & \frac{1}{L_{a,0}} \\ -b_{d,cc}k_{cc} & 0\end{bmatrix}$, $\boldsymbol{b}_{i_a} := \begin{bmatrix} k_{cc} & b_{d,cc}k_{cc}\end{bmatrix}^T$, $\boldsymbol{b}_{d_{i_a}} := \begin{bmatrix}\frac{1}{L_{a,0}} & 0\end{bmatrix}^T$, $\boldsymbol{c}_{i_a} := \begin{bmatrix} 1 & 0\end{bmatrix}$, $\tilde{d}_{i_a} := d_{i_a} - \hat{d}_{i_a}$, and dummy signal $r = 0$. The corresponding Laplace transform yields

$$\begin{aligned}Y_{i_a}(s) &= \boldsymbol{c}_{i_a}(s\boldsymbol{I}_{2\times 2} - \boldsymbol{A}_{i_a})^{-1}\boldsymbol{b}_{i_a}R(s)\\ &\quad +\boldsymbol{c}_{i_a}(s\boldsymbol{I}_{2\times 2} - \boldsymbol{A}_{i_a})^{-1}\boldsymbol{b}_{d_{i_a}}\tilde{D}_{i_a}(s),\end{aligned}$$

where

$$\boldsymbol{c}_{i_a}(s\boldsymbol{I}_{2\times 2} - \boldsymbol{A}_{i_a})^{-1}\boldsymbol{b}_{d_{i_a}} = \frac{s}{(s + k_{cc})(L_{a,0}s + b_{d,cc})}$$

and

$$\begin{aligned}\boldsymbol{c}_{i_a}(s\boldsymbol{I}_{2\times 2} - \boldsymbol{A}_{i_a})^{-1}\boldsymbol{b}_{i_a} &= \frac{k_{cc}(L_{a,0}s + b_{d,cc})}{(s + k_{cc})(L_{a,0}s + b_{d,cc})}\\ &= \frac{k_{cc}}{s + k_{cc}},\end{aligned}$$

due to the pole-zero cancellation, which can be written as (using the relationship $\frac{s}{L_{a,0}s+b_{d,cc}} = 1 - \frac{c_2}{s+c_1}$ for positive constants $c_1 := \frac{b_{d,cc}}{L_{a,0}^2}$ and $c_2 := \frac{b_{d,cc}}{L_{a,0}}$)

$$(s + k_{cc})Y_{i_a}(s) = k_{cc}R(s) + \tilde{D}_{i_a}(s) + \tilde{D}_{i_a,F}(s),\ \forall s \in \mathbb{C},$$

with $\tilde{D}_{i_a,F}(s) = -\frac{c_2}{s+c_1}\tilde{D}_{i_a}(s)$, confirming the result of this lemma by applying the inverse Laplace transform. ■

Now, it is ready to prove the exponential convergence behavior for the error $e_{cc} = i_a^* - i_a$ in Theorem 2.

Theorem 1: The proposed controller (11) guarantees

$$|e_{cc}| \leq \delta_{cc,1}e^{-\delta_{cc,2}t},\ \forall t \geq 0,$$

$\forall |\tilde{d}_{i_a}| \geq \frac{2M_{i_a}}{l_{i_a}}$, for some $\delta_{cc,i} > 0$, $i = 1, 2$, where $|\dot{d}_{i_a}| \leq M_{i_a}$, $\forall t \geq 0$. ♢

Proof: Define the vector $\boldsymbol{z}_{cc} := \begin{bmatrix} e_{cc} & \tilde{d}_{i_a,F}\end{bmatrix}^T$ leading to the system (using (17) and (18)) as

$$\dot{\boldsymbol{z}}_{cc} = \boldsymbol{A}_{cc}\boldsymbol{z}_{cc} + \boldsymbol{b}_{cc}\tilde{d}_{i_a},\ \forall t \geq 0, \tag{19}$$

where $\boldsymbol{A}_{cc} := \begin{bmatrix} -k_{cc} & 1 \\ 0 & -c_1\end{bmatrix}$ and $\boldsymbol{b}_{cc} := \begin{bmatrix} 1 \\ -c_2\end{bmatrix}$, which solves the matrix equation $\boldsymbol{A}_{cc}^T\boldsymbol{P}_{cc} + \boldsymbol{P}_{cc}\boldsymbol{A}_{cc} = -\boldsymbol{I}$ with respect to the unique solution $\boldsymbol{P}_{cc} > \boldsymbol{0}$ due to the stability of $\boldsymbol{A}_{cc}$. Consider the positive definite function:

$$V_{cc} := \frac{1}{2}\boldsymbol{z}_{cc}^T\boldsymbol{P}_{cc}\boldsymbol{z}_{cc} + \frac{\kappa_d}{2}\tilde{d}_{i_a},\ \kappa_d > 0,$$

whose time derivative is obtained using the closed-loop error dynamics (19) and DOB estimation dynamics (16) as

$$\begin{aligned}\dot{V}_{cc} &= \boldsymbol{z}_{cc}^T\boldsymbol{P}_{cc}(\boldsymbol{A}_{cc}\boldsymbol{z}_{cc} + \boldsymbol{b}_{cc}\tilde{d}_{i_a}) - \frac{\kappa_d l_{i_a}}{2}\tilde{d}_{i_a}^2\\ &\quad -\kappa_d(\frac{l_{i_a}}{2}\tilde{d}_{i_a}^2 - \dot{d}_{i_a}\tilde{d}_{i_a})\\ &\leq -\frac{1}{2}\|\boldsymbol{z}_{cc}\|^2 - (\frac{\kappa_d l_{i_a}}{2} - \frac{\|\boldsymbol{P}_{cc}\|^2\|\boldsymbol{b}_{cc}\|^2}{2})\tilde{d}_{i_a}^2,\\ &\quad \forall t \geq 0,\ \forall |\tilde{d}_{i_a}| \geq \frac{2M_{i_a}}{l_{i_a}},\end{aligned}$$

with the use of the Young's inequality ($\boldsymbol{x}^T\boldsymbol{y} \leq \frac{\epsilon}{2}\|\boldsymbol{x}\|^2 + \frac{1}{2\epsilon}\|\boldsymbol{y}\|^2$, $\forall \epsilon > 0$) to the inequality above. The coefficient $\kappa_d := \frac{2}{l_{i_a}}(\frac{\|\boldsymbol{P}_{cc}\|^2\|\boldsymbol{b}_{cc}\|^2}{2} + \frac{1}{2})$ shows that

$$\begin{aligned}\dot{V}_{cc} &\leq -\frac{1}{2}\|\boldsymbol{z}_{cc}\|^2 - \frac{1}{2}\tilde{d}_{i_a}^2\\ &\leq -\alpha_{cc}V_{cc}, \forall t \geq 0,\ \forall |\tilde{d}_{i_a}| \geq \frac{2M_{i_a}}{l_{i_a}},\end{aligned} \tag{20}$$

where $\alpha_{cc} := \{\frac{1}{\lambda_{min}(\boldsymbol{P}_{cc})}, \frac{1}{\kappa_d}\}$ ($\lambda_{min}(\boldsymbol{P}_{cc})$: minimum eigenvalue of $\boldsymbol{P}_{cc}$) and $|\dot{d}_{i_a}| \leq M_{i_a}$, $\forall t \geq 0$, which verifies the result due to the comparison principle in [18]. ■

From Theorem 1, the DOB gain satisfying $\frac{2M_{i_a}}{l_{i_a}} \approx 0$ (assumed in the following analysis) concludes the exponential convergence $i_a \to i_a^*$ due to the inequality

$$\dot{V}_{cc} \leq -\alpha_{cc}V_{cc} < 0,\ \forall t \geq 0,$$

This also shows the convergence $i_a \rightarrow i_{a,ref}$, exponentially, due to Lemma 1. Theorem 2 proves this convergence property.

Theorem 2: The proposed controller (11) guarantees

$$|\tilde{i}_a| \leq b_1 e^{-b_2 t},\ \forall t \geq 0,\ \forall |\tilde{i}_a| \geq \frac{2\kappa}{\hat{\omega}_{cc}},$$

for some $b_i > 0$, $i = 1, 2$, where $|\dot{i}_{a,ref}| \leq \kappa$, $\forall t \geq 0$. ◊

Proof: The error $\tilde{i}_a := i_{a,ref} - i_a$ satisfies $\tilde{i}_a = \tilde{i}_a^* + e_{cc}$ whose dynamics are obtained as (using (8), (17), and (18)):

$$\begin{aligned}\dot{\tilde{i}}_a &= -\hat{\omega}_{cc}\tilde{i}_a^* + \dot{i}_{a,ref} - k_{cc}e_{cc} + \tilde{d}_{i_a,F} + \tilde{d}_{i_a} \\ &= -\hat{\omega}_{cc}\tilde{i}_a + \boldsymbol{c}_{cc}^T \boldsymbol{z}_{cc} + \dot{i}_{a,ref},\end{aligned}$$

$\forall t \geq 0$, with $\boldsymbol{c}_{cc} := \begin{bmatrix}(\hat{\omega}_{cc} - k_{cc})\ 1\ 1\end{bmatrix}^T$ and application of the relationship $\tilde{i}_a^* = \tilde{i}_a - e_{cc}$ ($\Leftrightarrow \tilde{i}_a = \tilde{i}_a^* + e_{cc}$) to the last equation above, which renders the composite-type Lyapunov function candidate

$$V := \frac{1}{2}\tilde{i}_a^2 + \eta V_{cc},\ \eta > 0,\ \forall t \geq 0,$$

to be

$$\dot{V} = \tilde{i}_a(-\hat{\omega}_{cc}\tilde{i}_a + \boldsymbol{c}_{cc}^T \boldsymbol{z}_{cc} + \dot{i}_{a,ref}) + \eta \dot{V}_{cc},$$

with its upper bound (using (20))

$$\begin{aligned}\dot{V} &\leq -\frac{\omega_{cc}}{4}\tilde{i}_a^2 + \frac{c_{cc,max}^2}{\omega_{cc}}\|\boldsymbol{z}_{cc}\|^2 - \eta\alpha_{cc}V_{cc} \\ &\quad -(\frac{\hat{\omega}_{cc}}{2} - \frac{\kappa}{|\tilde{i}_a|})\tilde{i}_a^2 \\ &\leq -\frac{\omega_{cc}}{4}\tilde{i}_a^2 - (\eta\alpha_{cc} - \frac{2c_{cc,max}^2}{\omega_{cc}})V_{cc}, \\ &\quad \forall t \geq 0,\ \forall |\tilde{i}_a| \geq \frac{2\kappa}{\hat{\omega}_{cc}},\end{aligned}$$

where the property $\hat{\omega}_{cc} \geq \omega_{cc}$ (Lemma 2) and Young's inequality verify the first inequality above and $|\dot{i}_{a,ref}| \leq \kappa$ and $||\boldsymbol{c}_{cc}|| \leq c_{cc,max}, \forall t \geq 0$. The coefficient $\eta := \frac{1}{\alpha_{cc}}(\frac{2c_{cc,max}^2}{\omega_{cc}} + 1)$ leads to:

$$\dot{V} \leq -\alpha V,\ \forall t \geq 0,\ \forall |\tilde{i}_a| \geq \frac{2\kappa}{\hat{\omega}_{cc}},$$

with $\alpha := \min\{\omega_{cc}, \frac{1}{\eta}\}$, which completes the proof with the use of the comparison principle in [18]. ■

Note that the time-varying cut-off frequency boosting property ($\hat{\omega}_{cc} \geq \omega_{cc}, \forall t \geq 0$, depicted in Lemma 2) provides a rationale to assume that $\frac{2\kappa}{\hat{\omega}_{cc}} \approx 0$ so that

$$\dot{V} \leq -\alpha V,\ \forall t \geq 0, \tag{21}$$

which is used for the remaining analysis.

B. COMPLETE CLOSED-LOOP SYSTEM ANALYSIS

This section proves the proposed solution attains the control objective by showing the exponential convergence $\omega \rightarrow \omega^*$ using the inner loop system analysis result given as inequality (21). First, Lemma 5 derives the inherent pole-zero cancellation characteristic of the outer loop.

Lemma 5: The proposed controller (7) forces the outer loop dynamics to be the first-order system:

$$\dot{\omega}_m = \omega_{sc}\tilde{\omega}_m - k_{T,0}\tilde{i}_a + \tilde{i}_{a,F} + d_{\omega_m,F}, \tag{22}$$

with filtered signals such that

$$\dot{\tilde{i}}_{a,F} = -c_{sc,1}\tilde{i}_{a,F} - c_{sc,2}\tilde{i}_a, \tag{23}$$

$$J_{m,0}\dot{d}_{\omega_m,F} = -b_{d,sc}d_{\omega_m,F} + \Delta\dot{d}_{\omega_m},\ \forall t \geq 0, \tag{24}$$

for some positive constants $c_{sc,i}$, $i = 1, 2$, where Δd_{ω_m} represents the AC component of the disturbance d_{ω_m}. i.e., $d_{\omega_m} = d_{\omega_m,0}$ (DC) $+ \Delta d_{\omega_m}$ (AC). ◊

Proof: The closed-loop outer loop dynamics obtained from the substitution of (7) into (3) are given as the state-space representation for the state $\boldsymbol{x}_{\omega_m} := \begin{bmatrix}\omega_m\ \sigma_{\omega_m}\end{bmatrix}^T$ ($\sigma_{\omega_m} := b_{d,sc}\omega_{sc}\int_0^t \tilde{\omega}_m d\tau$) and output $y_{\omega_m} = \omega_m$ as

$$\begin{aligned}\dot{\boldsymbol{x}}_{\omega_m} &= \boldsymbol{A}_{\omega_m}\boldsymbol{x}_{\omega_m} + \boldsymbol{b}_{\omega_m}\omega_{m,ref} + \boldsymbol{b}_{d_\omega}(-k_{T,0}\tilde{i}_a + d_{\omega_m}), \\ y_{\omega_m} &= \boldsymbol{c}_{\omega_m}\boldsymbol{x}_{\omega_m},\ \forall t \geq 0,\end{aligned}$$

with $\boldsymbol{A}_{\omega_m} := \begin{bmatrix}-\frac{(b_{d,sc}+J_{m,0}\omega_{cc})}{J_{m,0}} & \frac{1}{J_{m,0}} \\ -b_{d,sc}\omega_{sc} & 0\end{bmatrix}$, $\boldsymbol{b}_{\omega_m} := \begin{bmatrix}\omega_{sc}\ b_{d,sc}\omega_{sc}\end{bmatrix}^T$, $\boldsymbol{b}_{d_\omega} := \begin{bmatrix}\frac{1}{J_{m,0}}\ 0\end{bmatrix}^T$, and $\boldsymbol{c}_{\omega_m} := \begin{bmatrix}1\ 0\end{bmatrix}$. The corresponding Laplace transform yields

$$\begin{aligned}Y_{\omega_m}(s) &= \boldsymbol{c}_{\omega_m}(s\boldsymbol{I}_{2\times 2} - \boldsymbol{A}_{\omega_m})^{-1}\boldsymbol{b}_{\omega_m}\Omega_{m,ref}(s) \\ &\quad + \boldsymbol{c}_{\omega_m}(s\boldsymbol{I}_{2\times 2} - \boldsymbol{A}_{\omega_m})^{-1}\boldsymbol{b}_{d_\omega}(-k_{T,0}\tilde{I}_a(s) \\ &\quad + D_{\omega_m}(s)),\ \forall s \in \mathbb{C},\end{aligned}$$

where

$$\boldsymbol{c}_{\omega_m}(s\boldsymbol{I}_{2\times 2} - \boldsymbol{A}_{\omega_m})^{-1}\boldsymbol{b}_{d_\omega} = \frac{s}{(s+\omega_{sc})(J_{m,0}s + b_{d,sc})}$$

and

$$\begin{aligned}\boldsymbol{c}_{\omega_m}(s\boldsymbol{I}_{2\times 2} - \boldsymbol{A}_{\omega_m})^{-1}\boldsymbol{b}_{\omega_m} &= \frac{\omega_{sc}(J_{m,0}s + b_{d,sc})}{(s+\omega_{sc})(J_{m,0}s + b_{d,sc})} \\ &= \frac{\omega_{sc}}{s+\omega_{sc}},\end{aligned}$$

due to the pole-zero cancellation, which can be written as (using the relationship $\frac{s}{J_{m,0}s + b_{d,sc}} = 1 - \frac{b_2}{s+b_1}$ for positive constants $b_1 := \frac{b_{d,sc}}{J_{m,0}^2}$ and $b_2 := \frac{b_{d,sc}}{J_{m,0}}$)

$$\begin{aligned}(s+\omega_{sc})Y_{\omega_m}(s) &= \omega_{sc}\Omega_{m,ref}(s) - k_{T,0}\tilde{I}_a(s) + \tilde{I}_{a,F}(s) \\ &\quad + \frac{s}{(J_{m,0}s + b_{d,sc})}D_{\omega_m}(s),\ \forall s \in \mathbb{C},\end{aligned}$$

with $E_{cc,F}(s) = \frac{k_{T,0}b_2}{s+b_1}E_{cc}(s)$, which confirms the result of this lemma after applying the inverse Laplace transform. ■

The subtraction of (22)-(24) from the target system (5) gives the error dynamics with respect to the error $e_{sc} := \omega_m^* - \omega_m$ as

$$\dot{e}_{sc} = -\omega_{sc} e_{sc} - \tilde{i}_{a,F} - d_{\omega_m,F} + k_{T,0}\tilde{i}_a, \ \forall t \geq 0, \quad (25)$$

which is used to confirm the control objective accomplishment by showing the exponential convergence $\omega_m \to \omega_m^*$ in Theorem 3 together with inequality (21).

Theorem 3: The control system depicted in Fig. 1 guarantees

$$|e_{sc}| \leq \delta_{sc,1} e^{-\delta_{sc,2} t}, \ \forall t \geq 0, \ \forall |d_{\omega_m,F}| \geq \frac{2M_{\omega_m}}{b_{d,sc}},$$

for some $\delta_{sc,i} > 0$, $i = 1, 2$, where $|\Delta \dot{d}_{\omega_m}| \leq M_{\omega_m}$, $\forall t \geq 0$. ◊

Proof: Define the vector $\boldsymbol{z}_{sc} := \begin{bmatrix} e_{sc} & \tilde{i}_{a,F} \end{bmatrix}^T$ leading to the system (using (23)-(25) as

$$\dot{\boldsymbol{z}}_{sc} = \boldsymbol{A}_{sc}\boldsymbol{z}_{sc} + \boldsymbol{b}_{sc,1}\tilde{i}_a + \boldsymbol{b}_{sc,2} d_{\omega_m,F}, \ \forall t \geq 0, \quad (26)$$

where $\boldsymbol{A}_{sc} := \begin{bmatrix} -\omega_{sc} & -1 \\ 0 & -c_{sc,1} \end{bmatrix}$, $\boldsymbol{b}_{sc,1} := \begin{bmatrix} k_{T,0} \\ -c_{sc,2} \end{bmatrix}$, and $\boldsymbol{b}_{sc,2} := \begin{bmatrix} -1 \\ 0 \end{bmatrix}$, which solves the matrix equation $\boldsymbol{A}_{sc}^T \boldsymbol{P}_{sc} + \boldsymbol{P}_{sc}\boldsymbol{A}_{sc} = -\boldsymbol{I}$ with respect to the unique solution $\boldsymbol{P}_{sc} > \boldsymbol{0}$ due to the stability of $\boldsymbol{A}_{sc}$. Consider the positive definite function:

$$V_{sc} := \frac{1}{2}\boldsymbol{z}_{sc}^T \boldsymbol{P}_{sc}\boldsymbol{z}_{sc} + \frac{\zeta_d J_{m,0}}{2} d_{\omega_m,F}^2 + \zeta_v V, \ \forall t \geq 0,$$

with positive coefficients $\zeta_d > 0$ and $\zeta_v > 0$, whose time derivative is obtained using the dynamics (26) and (24) as

$$\begin{aligned} \dot{V}_{sc} &= \boldsymbol{z}_{sc}^T \boldsymbol{P}_{sc}(\boldsymbol{A}_{sc}\boldsymbol{z}_{sc} + \boldsymbol{b}_{sc,1}\tilde{i}_a + \boldsymbol{b}_{sc,2} d_{\omega_m,F}) \\ &\quad + \zeta_d d_{\omega_m,F}(-b_{d,sc} d_{\omega_m,F} + \Delta \dot{d}_{\omega_m}) + \zeta_v \dot{V} \\ &\leq -\frac{1}{3}\|\boldsymbol{z}_{sc}\|^2 - \left(\frac{\zeta_d b_{d,sc}}{2} - \frac{3\|\boldsymbol{P}_{sc}\|^2 \|\boldsymbol{b}_{sc,2}\|^2}{4}\right) d_{\omega_m,F}^2 \\ &\quad - \left(\zeta_v \alpha - \frac{3\|\boldsymbol{P}_{sc}\|^2 \|\boldsymbol{b}_{sc,1}\|^2}{2}\right) V \\ &\quad - \zeta_d \left(\frac{b_{d,sc}}{2} d_{\omega_m,F}^2 - \Delta \dot{d}_{\omega_m} d_{\omega_m,F}\right), \ \forall t \geq 0, \end{aligned}$$

with the use of the Young's inequality to the inequality above. The coefficients $\zeta_d := \frac{2}{b_{d,sc}}\left(\frac{3\|\boldsymbol{P}_{sc}\|^2 \|\boldsymbol{b}_{sc,2}\|^2}{4} + \frac{1}{2}\right)$ and $\zeta_v := \frac{1}{\alpha}\left(\frac{3\|\boldsymbol{P}_{sc}\|^2 \|\boldsymbol{b}_{sc,1}\|^2}{2} + 1\right)$ show that

$$\begin{aligned} \dot{V}_{sc} &\leq -\frac{1}{3}\|\boldsymbol{z}_{sc}\|^2 - \frac{1}{2} d_{\omega_m,F}^2 - V, \\ &\leq -\alpha_{sc} V_{sc}, \ \forall t \geq 0, \ \forall |d_{\omega_m,F}| \geq \frac{2M_{\omega_m}}{b_{d,sc}}, \end{aligned}$$

where $\alpha_{sc} := \min\left\{\frac{2}{3\lambda_{min}(\boldsymbol{P}_{sc})}, \frac{1}{\zeta_d J_{m,0}}, \frac{1}{\zeta_v}\right\}$ ($\lambda_{min}(\boldsymbol{P}_{sc})$: minimum eigenvalue of $\boldsymbol{P}_{sc}$) and $|\Delta \dot{d}_{\omega_m}| \leq M_{\omega_m}$, $\forall t \geq 0$, which completes the proof with the use of the comparison principle in [18]. ■

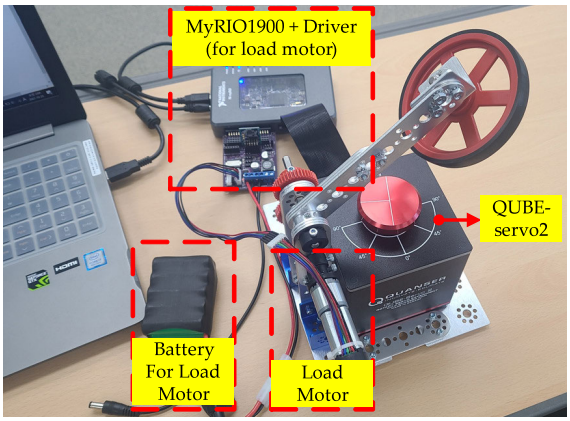

FIGURE 2. Experimental platform comprising QUBE-servo2 and myRIO-1900 processor.

Theorem 3 reveals the role of active damping depressing the high-frequency component of the disturbance, concluding that the proposed controller depicted in Fig. 1 accomplishes the control objective by ensuring the exponential convergence

$$\lim_{t \to \infty} \omega = \omega^*$$

under the condition $\frac{2M_{\omega_m}}{b_{d,sc}} \approx 0$.

V. EXPERIMENTAL RESULTS

Fig. 2 presents the experimental platform based on the QUBE-servo2 and myRIO-1900 processor using Simulink/MATLAB for the gain tuning process and resulting data collection. In this platform, the load motor applies the load torque to the QUBE servo2 through the closed-loop angle control implemented by the MyRIO-1900. The true system parameters and their nominal version are given by: $J_m = 4 \times 10^{-6}$ kgm^2, and $B_m = 4 \times 10^{-7}$ Nm/(rad/s), $R_a = 8.4\ \Omega$, $L_a = 1.16$ mH, $k_T = 0.042$ Nm/A, $k_e = 0.042$ V/(rad/s), $J_{m,0} = 0.7J_m$, and $B_{m,0} = 1.1B_m$, $R_{a,0} = 0.8R_a$, $L_{a,0} = 1.2L_a$, and $k_{T,0} = k_{e,0} = 1.3k_T$, with the control period 0.1 ms.

The tuning result of the proposed controller is, for the inner loop, (variable cut-off frequency) $f_{cc} = 10$ Hz ($\omega_{cc} = 2\pi 10$ rad/s), $\gamma_{cc} = 2 \times 10^7$, $\rho_{cc} = 10/\gamma_{cc}$, (control) $k_{cc} = 1000$, $b_{d,cc} = 20$, (DOB) $l_{i_a} = 1900$, and, for the outer loop, $f_{sc} = 2$ Hz ($\omega_{sc} = 2\pi 2$ rad/s) and $b_{d,cc} = 0.3$.

This section highlights the effectiveness of the variable current cut-off frequency update rule (primary contribution of this study) with a comparison study by activating and deactivating the update rule (9) in the speed-tracking and regulation tasks.

A. SPEED-TRACKING TASK

This section uses the pulse speed reference with its minimum and maximum values of 500 and 1500 rpm to evaluate speed tracking performance. Fig. 3 demonstrates the practical merit of the proposed controller subject to the current

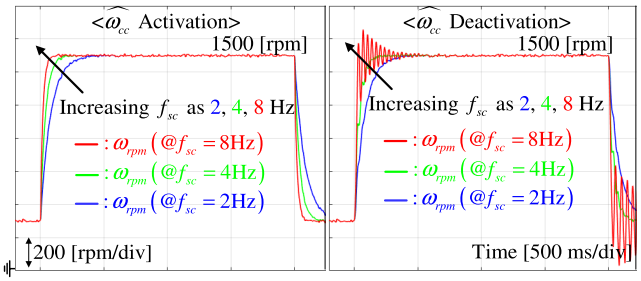

FIGURE 3. Speed response comparison under pulse speed reference-tracking task as increasing f_{sc} = 2, 4, and 8 Hz.

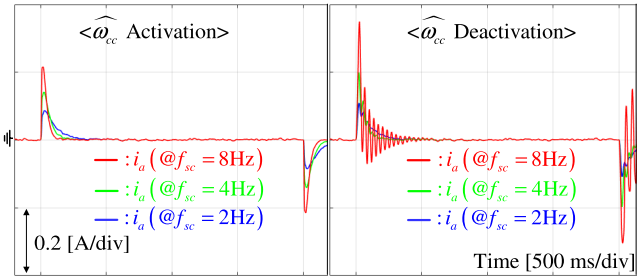

FIGURE 4. Stator current response comparison under pulse speed reference-tracking task as increasing f_{sc} = 2, 4, and 8 Hz.

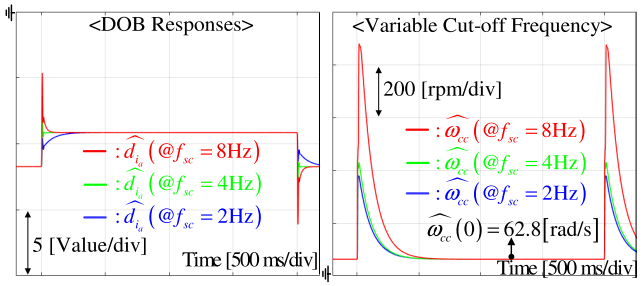

FIGURE 5. DOB and variable cut-off frequency responses under pulse speed reference-tracking task as increasing f_{sc} = 2, 4, and 8 Hz.

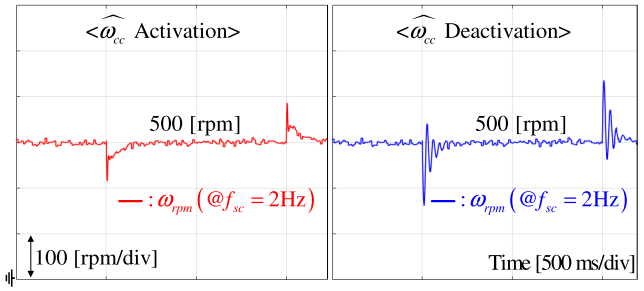

FIGURE 6. Speed response comparison under abrupt load torque variation at 500 rpm operation mode.

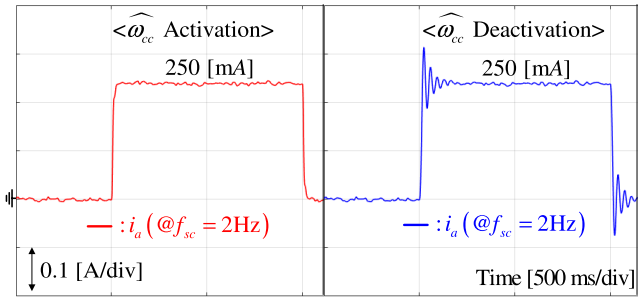

FIGURE 7. Stator current comparison under abrupt load torque variation at 500 rpm operation mode.

cut-off frequency boosting property indicated in the right panel of Fig. 5. Particularly, the proposed controller successfully maintained the desired speed tracking performance by increasing the speed cut-off frequency (f_{sc} = 2, 4, and 8 Hz) without any performance degradation (such as oscillation) owing to the current cut-off frequency boosting nature shown in the right panel of Fig. 5. The deactivation of the proposed variable cut-off frequency mechanism failed to make the increased speed cut-off frequency feasible, involving considerable speed oscillations for the cases of f_{sc} = 4 and 8 Hz, which would be alleviated by constantly increasing the current cut-off frequency f_{cc}. These observations are summarized as: (a) feasible speed bandwidth expansion and (b) lowered current cut-off frequency in steady-state operation. Fig. 4 shows the corresponding stator current behaviors where the proposed controller stabilizes the current more rapidly than when deactivating the variable cut-off frequency update mechanism. The left panel of Fig. 5 presents the estimated disturbance responses from the DOB.

B. SPEED REGULATION TASK

1) TRANSIENT RESPONSE COMPARISON

This section fixes the speed reference to 500 rpm to evaluate the speed maintenance performance while abruptly applying and removing the load torque, causing the current peak level increment (approximately 250 mA) depicted in Fig. 7. Fig. 6 depicts the resultant speed responses whose over/under shoots and oscillation periods are effectively suppressed by the proposed controller boosting the cut-off frequency of the current-loop.

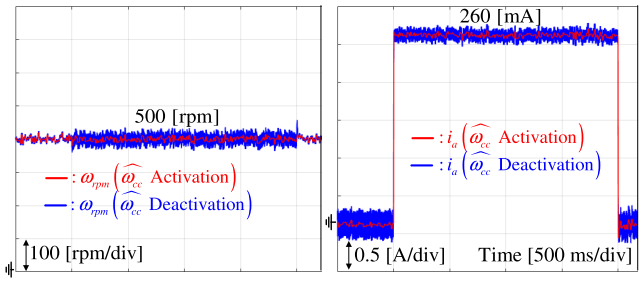

FIGURE 8. Steady-state speed response comparison under pulse speed reference-tracking task.

2) STEADY-STATE RESPONSE COMPARISON

Under the same setting as the previous subsection, only the initial current cut-off frequency was increased to f_{cc} = 300 Hz (so that $\hat{\omega}_{cc}(0) = 2\pi 300$ rad/s) for the case of

deactivating the update rule (9) to improve the closed-loop performance without using the variable current cut-off frequency mechanism. In contrast, the proposed controller uses the original initial current cut-off frequency value $f_{cc} = 10$ Hz, (so that $\hat{\omega}_{cc}(0) = 62.8$ rad/s). As expected, Fig. 8 shows that the use of a constantly increasing current cut-off frequency considerably magnifies the current ripple level but the proposed variable cut-off frequency mechanism successfully avoids this demerit by decreasing the cut-off frequency value to its initial value by reaching the steady-state. This practical benefit increases the power efficiency by switching loss reduction for large power system applications.

VI. CONCLUSION

In this study, a variable cut-off frequency mechanism was designed to enlarge the feasible speed operation region with a convergence analysis, including experimental verification. From the experimental study, the proposed controller accomplished the two main objectives; making the high speed cut-off frequency feasible and lowering the steady-state cut-off frequency value (leading to the current ripple reduction). An offline optimization process will be established under linear or bilinear matrix constraints to determine the optimal controller design parameters in a future study involving three-phase motor applications.

REFERENCES

[1] H. Yan, W. Zhao, G. Buticchi, and C. Gerada, "Active thermal control for modular power converters in multi-phase permanent magnet synchronous motor drive system," *IEEE Access*, vol. 9, pp. 7054–7063, 2021.

[2] S. Fu, H. Ren, T. Lin, S. Zhou, Q. Chen, and Z. Li, "SM-PI control strategy of electric motor-pump for pure electric construction machinery," *IEEE Access*, vol. 8, pp. 100241–100250, 2020.

[3] K. R. Khan and M. S. Miah, "Fault-tolerant BLDC motor-driven pump for fluids with unknown specific gravity: An experimental approach," *IEEE Access*, vol. 8, pp. 30160–30173, 2020.

[4] C. R. Lee, S.-K. Kim, and C. K. Ahn, "Auto-tuning proportional-type synchronization algorithm for DC motor speed control applications," *IEEE Trans. Circuits Syst. II, Exp. Briefs*, vol. 67, no. 3, pp. 521–525, Mar. 2020.

[5] Y. Kim, S.-K. Kim, and C. K. Ahn, "Variable cut-off frequency observer-based positioning for ball-beam systems without velocity and current feedback considering actuator dynamics," *IEEE Trans. Circuits Syst. I, Reg. Papers*, vol. 68, no. 1, pp. 396–405, Jan. 2021.

[6] Y. I. Son, I. H. Kim, D. S. Choi, and H. Shim, "Robust cascade control of electric motor drives using dual reduced-order PI observer," *IEEE Trans. Ind. Electron.*, vol. 62, no. 6, pp. 3672–3682, Jun. 2015.

[7] S.-K. Kim and C. K. Ahn, "DC motor speed regulator via active damping injection and angular acceleration estimation techniques," *IEEE/CAA J. Autom. Sinica*, vol. 8, no. 3, pp. 641–647, Mar. 2021.

[8] S.-K. Sul, *Control of Electric Machine Drive Systems*, vol. 88. Hoboken, NJ, USA: Wiley, 2011.

[9] C. Olalla, R. Leyva, I. Queinnec, and D. Maksimovic, "Robust gain-scheduled control of switched-mode DC–DC converters," *IEEE Trans. Power Electron.*, vol. 27, no. 6, pp. 3006–3019, Jun. 2012.

[10] H. Ahmed, M. Ahsan, M. Benbouzid, A. Albarbar, M. Shahjalal, and S. Biricik, "Coordinate transformation-free observer-based adaptive estimation of distorted single-phase grid voltage signal," *IEEE Access*, vol. 8, pp. 74280–74290, 2020.

[11] R. M. Asl, R. Palm, H. Wu, and H. Handroos, "Fuzzy-based parameter optimization of adaptive unscented Kalman filter: Methodology and experimental validation," *IEEE Access*, vol. 8, pp. 54887–54904, 2020.

[12] Y. Chen, Z. Ming, and M. Menenti, "Change detection algorithm for multi-temporal remote sensing images based on adaptive parameter estimation," *IEEE Access*, vol. 8, pp. 106083–106096, 2020.

[13] M. Takizawa and M. Yukawa, "Joint learning of model parameters and coefficients for online nonlinear estimation," *IEEE Access*, vol. 9, pp. 24026–24040, 2021.

[14] L. Liu, Y. J. Liu, and C. L. P. Chen, "Adaptive neural network control for a DC motor system with dead-zone," *Nonlinear Dyn.*, vol. 72, no. 1, pp. 141–147, 2013.

[15] J. Yao, Z. Jiao, and D. Ma, "Adaptive robust control of DC motors with extended state observer," *IEEE Trans. Ind. Electron.*, vol. 61, no. 7, pp. 3630–3637, Jul. 2014.

[16] A. A. El-samahy and M. A. Shamseldin, "Brushless DC motor tracking control using self-tuning fuzzy PID control and model reference adaptive control," *Ain Shams Eng. J.*, vol. 9, no. 3, pp. 341–352, Sep. 2018.

[17] J. K. Park, J.-H. Lee, S.-K. Kim, and C. K. Ahn, "Output-feedback speed-tracking control without current feedback for BLDCMs based on active-damping and invariant surface approach," *IEEE Trans. Circuits Syst. II, Exp. Briefs*, vol. 68, no. 7, pp. 2528–2532, Jul. 2021.

[18] H. K. Khalil, *Nonlinear Systems*. Upper Saddle River, NJ, USA: Prentice-Hall, 2002.

SUNG HYUN YOU received the B.S. degree in electrical engineering from the Seoul National University of Science and Technology, Seoul, South Korea, in 2013, and the Ph.D. degree from the School of Electrical Engineering, Korea University, Seoul, in 2019. He was a Research Professor at the Research Institute of Engineering and Technology, Korea University. Since 2020, he has been an Assistant Professor at Chosun University, South Korea. His research interests include optimal, robust, intelligent, and receding horizon control and estimation.

YEON JI is currently pursuing the M.S. degree in creative convergence engineering with Hanbat National University, Daejeon, South Korea. Her research interests include the state estimation and stabilization algorithms for unstable systems, such as balancing robot, inverted pendulum, and quadcopter, and their implementations using various micro(digital signal)-processors.

SEOK-KYOON KIM received the B.S. degree in electronic and IT media engineering from the Seoul National University of Science and Technology, Seoul, South Korea, in 2004, and the Ph.D. degree in electrical engineering from Korea University, Seoul, in 2014.

He worked as a Senior Research Engineer at LG Electronics, from 2015 to 2016, and joined the Department of Creative Convergence Engineering, Hanbat National University, Daejeon, South Korea, in 2017. His research interests include the tracking problem of power electronic applications such as power converters and motor drive, the power system stabilization problem, and the development of control theory such as passivity-based control and nonlinear adaptive control.